

CONTENTS

S1 Handedness and magnetic point groups	2
S2 Stereographic projection	2
S3 Symmetry considerations on optically induced Faraday/Kerr rotation	4
S4 Elliptical third-harmonic Generation – classical/macroscopic derivation based on magnetic point groups	9
S5 Optical Stark and Bloch-Siegert shifts with elliptical polarization	13
S6 Quantum-mechanical model for third-harmonic Generation	15
General analytical expression for the $\chi^{(3)}$ tensor of a solid	15
Model Hamiltonian for monolayer TMDs	16
Evaluating $\chi^{(3)}$ for a monolayer TMD	17
Evaluation of the third-harmonic rotation from the $\chi^{(3)}$ tensor	19
Model Hamiltonian for bilayer TMDs	20
Evaluating $\chi^{(3)}$ for bilayer TMDs	22
Evaluation of the third-harmonic rotation from the $\chi^{(3)}$ tensor	24
S7 Exemplary polar plots of the fundamental and third-harmonic beams	25
S8 Nonlinear Faraday rotation for Mo based TMDs	25
S9 Comparison linear transmittance and third-harmonic wavelength dependence	26
References	26

S1 HANDEDNESS AND MAGNETIC POINT GROUPS

To understand the symmetry operations that define the time-invariant and time-noninvariant terms of the NLO susceptibilities in mono- and bilayer TMDs, we first need to discuss the property of *handedness* of spin-oriented states. As an example, we take a rotating sphere. The sphere possesses the binary property of *handedness*: it rotates either right (clockwise or \downarrow) or left (counter-clockwise or \uparrow). When the rotating sphere is mirrored with respect to a plane perpendicular to the axis of rotation, the rotation direction remains unchanged. Thus, this horizontal reflection is a symmetry operation. Instead, for mirror operations along any plane that contains the axis of rotation, the rotation direction changes sign [1]. This vertical reflection can be considered as a symmetry operation only in combination with a flip of the rotation direction, *i.e.*, an antisymmetry operation [2]. Note that in crystals horizontal and vertical mirror planes are typically defined as perpendicular and parallel to the main axis of rotation, respectively. In general, symmetry operations within a unit cell of a crystal can be grouped into five categories: identity, proper rotation, reflection, inversion and roto-reflection. By combining these symmetry operations, one can derive the **crystallographic** point groups, which ultimately define the NLO properties of crystals as long as TRS is preserved [3]. Following the discussion above, we can now consider a binary information on each site of the unit cell, such as the electron spin. This binary property can be reversed by the antisymmetry operation, *i.e.* by changing spin up to spin down (or analogously by changing *black* into *white* [2]). Combining **crystallographic** point groups with this binary property defines the **magnetic** (*black* and *white*) point groups. These are fundamental to describe crystal properties upon breaking of TRS [4].

S2 STEREOGRAPHIC PROJECTION

In this section, we discuss the stereographic projection that we use in the main text to identify symmetry operations for crystallographic point groups and magnetic groups in TMDs. Relevant symmetry operations and their stereographic projections are shown in Fig. S1, while a more detailed explanation can be found, *e.g.*, in Ref. [5].

We show six exemplary symmetry operations: horizontal mirror (Fig. S1a), vertical mirror (Fig. S1b), C_2 rotation (rotation along vertical axis vector, Fig. S1c), n -fold rotational sym-

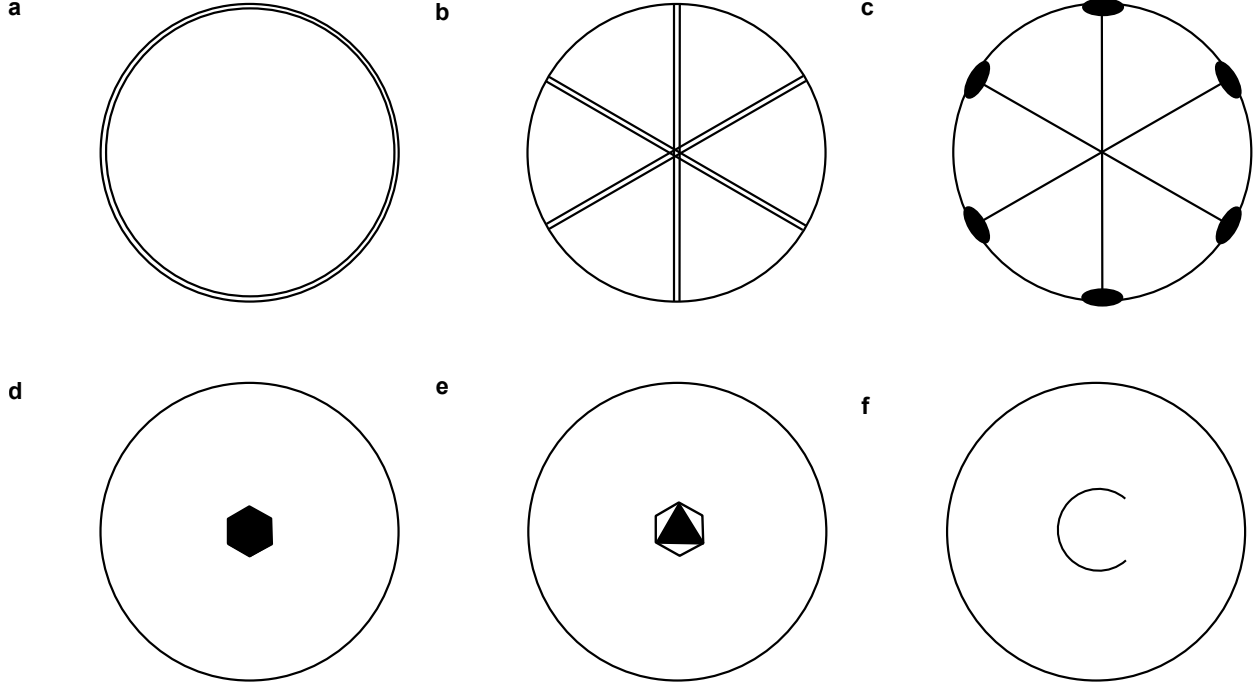


Fig. S1: **Stereographic projection of different point symmetry operations.** Each element **a** to **f** represents the stereographic projection of a specific symmetry operation. **a** Horizontal mirror. **b** Vertical mirror. **c** C_2 operation, *i.e.*, two-fold rotation along a vertical axis. **d** n -fold rotation (here $n = 6$). **e** n -fold rotoinversion (here $n = 6$). **f** Roto-inversion (rotation combined with inversion).

metry (here 6-fold, Fig. S1d), n -fold rotoinversion symmetry (Fig. S1e) and roto-inversion (Fig. S1f). One can combine the given symmetry operations into one single stereographic projection to obtain the graphs shown in Fig. 2b, e, h and k of the main text. For example, a TMD monolayer with preserved TRS belongs to the $\bar{6}m2$ symmetry group, and thus the allowed symmetry operations are (Fig. 2b of the main text): one horizontal mirror, three vertical mirrors, 3-fold rotation symmetry, and three C_2 rotations (two-fold rotations). When TRS is broken, the symmetry of monolayer TMDs is reduced to the magnetic group $\bar{6}m'2'$, and some symmetry operations are allowed only in combination with the antisymmetry operation (Fig. 2e of the main text): C_2 rotations and vertical mirror planes are thus depicted in red. A similar situation appears in TMD bilayers, that belong to the $\bar{3}m$ group (Fig. 2h of the main text) when TRS is preserved. Here, the symmetry operations are: three C_2 rotations, three vertical mirrors, 3-fold rotation symmetry and roto-inversion. When TRS is broken, the symmetry of TMD bilayers is reduced to the $\bar{3}m'$ magnetic group (Fig. 2k

of the main text), where only the 3-fold rotation symmetry and roto-inversion are allowed without the antisymmetry operation.

S3 SYMMETRY CONSIDERATIONS ON OPTICALLY INDUCED FARADAY/KERR ROTATION

The all-optically induced broken TRS and consequent Faraday/Kerr rotation can be understood based on symmetry considerations (*i.e.*, a macroscopic approach) by recalling the Curie principle, which states that an external perturbation reduces the symmetry of a system, allowing only those symmetry operations that are common to both the unperturbed system and the perturbation. Therefore, the new (reduced) symmetry group of the perturbed system can only be a subgroup of the original (unperturbed) symmetry group [5, 6].

Building on this principle and considering that in our experiments TRS breaking occurs *via* excitation of the sample with circularly polarized light, we can derive a table of how a nonmagnetic point group can “transform” into a magnetic point group. The perturbation must reduce the symmetry of the unperturbed crystal by removing some symmetry operations, which become allowed only if combined with the antisymmetry (AS) operation. In our case, the perturbation is circularly polarized light which, due to its intrinsic handedness, prohibits mirror operations along any plane that contains the propagation axis of the light beam, as well as C_2 rotations perpendicular to the propagation axis of the light beam.

Assuming a light beam that propagates along the main rotation axis of the crystal, in Table 1 we highlight if vertical mirror (mirror plane parallel to the main axis of rotation of the crystal) and C_2 rotation (perpendicular to the main axis of rotation of the crystal) are allowed in the initial point group and, subsequently, in the magnetic point group obtained by breaking TRS with circularly polarized light. While doing this, we further consider that from the 122 existing magnetic point groups, only 31 are admissible by symmetry consideration on possible spin orientations [7, 8]. Finally, in the last column we check if the initial point group (unperturbed crystal) and the subsequent allowed magnetic point group (crystal+light) have the same non-zero elements of the third order nonlinear susceptibility tensor $\chi^{(3)}$.

It is interesting to note that the point groups 2, m , $2/m$ and $mm2$ have two admissible magnetic point groups, depending on the spin orientation. From Table 1, we can divide the

Table 1. Comparison of the allowed symmetry operations and $\chi^{(3)}$ tensor for all the admissible non-magnetic and magnetic point groups. AS in the table means that the symmetry operation is allowed only in combination with the antisymmetry (AS) operation.

Point group (unperturbed crystal)	vertical mirror, plane parallel to main rotation axis	C ₂ rotation perpendicu lar to main rotation axis	Allowed magnetic point group* (crystal + light)	vertical mirror, plane parallel to main rotation axis	C ₂ rotation perpendicu lar to main rotation axis	Same elements of $\chi^{(3)}$ tensor	
1	No	No	1	No	No	Yes	Class 1
$\bar{1}$	No	No	$\bar{1}$	No	No	Yes	
3	No	No	3	No	No	Yes	
$\bar{3}$	No	No	$\bar{3}$	No	No	Yes	
4	No	No	4	No	No	Yes	
$\bar{4}$	No	No	$\bar{4}$	No	No	Yes	
4/m	No	No	4/m	No	No	Yes	
6	No	No	6	No	No	Yes	
$\bar{6}$	No	No	$\bar{6}$	No	No	Yes	
6/m	No	No	6/m	No	No	Yes	
2**	No	Yes	2	No	Yes	Yes	Class 2
			2'	No	AS	No	
m***	Yes	No	m	Yes	No	Yes	
			m'	AS	No	No	
2/m**	No	Yes	2/m	No	Yes	Yes	
			2'/m'	No	AS	No	
mm2**	Yes	Yes	mm'2'	Yes	AS	No	Class 3
			m'm'2	AS	Yes	No	
222	No	Yes	2'2'2	No	AS	No	
mmm	Yes	Yes	m'm'm	AS	AS	No	
422	No	Yes	42'2'	No	AS	No	
4mm	Yes	No	4m'm'	AS	No	No	
4/mmm	Yes	Yes	4/mm'm'	AS	AS	No	
$\bar{4}2m$	Yes	Yes	$\bar{4}2m'$	AS	AS	No	
3m	Yes	No	3m'	AS	No	No	
$\bar{3}m$	Yes	Yes	$\bar{3}m'$	AS	AS	No	
32	No	Yes	32'	No	AS	No	
622	No	Yes	62'2'	No	AS	No	
6mm	Yes	No	6m'm'	AS	No	No	
6/mmm	Yes	Yes	6/mm'm'	AS	AS	No	
$\bar{6}m2$	Yes	Yes	$\bar{6}m'2'$	AS	AS	No	
432	No	Yes	None	-	-	-	Class 4
$\bar{4}3m$	Yes	No	None	-	-	-	
$m\bar{3}$	Yes	No	None	-	-	-	
$m\bar{3}m$	Yes	No	None	-	-	-	
23	No	Yes	None	-	-	-	

* Considering the 32 allowed magnetic point groups and the Curie principle.

** In these point groups, C₂ rotation is the only allowed rotational symmetry, and thus also the main axis of rotation. In this case, TRS breaking with circularly polarized light only occurs if the light beam propagates along a direction perpendicular to the C₂ rotation axis.

*** For the crystal class *m* there is only one mirror plane, which can be arbitrary defined as vertical or horizontal.

32 non-magnetic point groups into 4 classes:

Class 1 (10 point groups): If the unperturbed crystal belongs to a (non-magnetic) point group where vertical mirrors and C_2 rotations perpendicular to the axis of highest rotational symmetry are not allowed, then the transition to a magnetic point group will have no effect on the $\chi^{(3)}$ tensor. Namely, the $\chi^{(3)}$ tensor of the unperturbed crystals and that of the corresponding magnetic point group will be identical. For those point groups, it will not be possible to measure any rotation of the TH polarization with respect to the polarization of the fundamental beam upon breaking of TRS using circularly polarized light, and thus our method is not applicable. However, one might find signatures of broken TRS in a change of the amplitude of some elements of the $\chi^{(3)}$ tensor, rather than their “zerness”.

Class 2 (3 point groups): In this class of point groups, the $\chi^{(3)}$ tensor can either change or remain identical, depending on how the polarization direction of the circularly polarized light is aligned with the symmetry axes of the crystal. In the configuration where the $\chi^{(3)}$ tensor changes upon breaking of TRS, our method is applicable.

Class 3 (14 point groups): If the unperturbed crystal belongs to a point group where vertical mirror and C_2 rotations perpendicular to the axis of highest rotational symmetry are allowed, then breaking of TRS with circularly polarized light will remove those symmetries. For those point groups, the resulting $\chi^{(3)}$ tensor will be different compared to the one of the unperturbed crystals (*i.e.*, different non-zero elements). In other words, circularly polarized light always reduces the symmetry of the crystal (Curie principle) by removing those symmetry operations that are not compatible with a “rotating object”, namely mirror planes that contains the propagation axis of the light beam, and C_2 rotations perpendicular to the propagation axis of the light beam.

Class 4 (4 point groups): For point groups 432 , $\bar{4}3m$, $m3m$, 23 there are no admissible magnetic point groups. Namely, the set of symmetries that define these point groups are not compatible with any ferromagnetic state, not even when combined with the antisymmetry operation [8].

Next, we shall clarify why our method is suitable for all crystals belonging to the Class 2 and Class 3, namely we shall show that the differences in the $\chi^{(3)}$ tensor induced by the all-optical broken TRS are responsible for a rotation of the TH polarization. To do that, we notice that all crystals classes of Class 2 and Class 3 can be further grouped into four categories, where the $\chi^{(3)}$ tensor is identical for each category. In Table 2 we report the

non-zero elements of the $\chi^{(3)}$ tensor for each of those categories in both cases when TRS is either preserved or broken (data from Refs. [9] and [10]). For simplicity, we highlight only the “in-plane” elements of the NLO susceptibility (xy plane). This is equivalent to assuming that the light propagates along the axis of highest rotational symmetry, which is defined as the z axis in Refs. [9] and [10]. Further, we consider the paraxial approximation, which for our experimental conditions is well justified as the objective and lens that we employ for focussing the fundamental beam and collimating the emitted third-harmonic both have low numerical apertures.

From the elements of the $\chi^{(3)}$ reported in Table 2, one can analytically show that all-optical breaking of TRS with circularly polarized light leads to a rotation of the TH polarization. For instance, in section S3, we calculate the rotation angle when going from point groups $\bar{6}m2$ and $\bar{3}m$ (mono- and bilayer TMDs) to the magnetic point groups $\bar{6}m'2'$ and $\bar{3}m'$. Based on Table 2, the same equations are true for point groups 622 , $6mm$, $6/mmm$, $\bar{6}m2$ and 32 , $3m$, $\bar{3}m$. For the remaining non-magnetic point groups, one could simply observe that, in the case of an input FB polarized only along the x direction, the TH polarization will be emitted along the same direction: $P_x = \chi_{xxxx}^{(3)} E_x^3$, $P_y = P_z = 0$. In contrast, when breaking TRS, the same input polarization of the FB will lead to a rotation in the polarization of the emitted TH according to: $P_x = \chi_{xxxx}^{(3)} E_x^3$, $P_y = \chi_{yxxx}^{(3)} E_x^3$, $P_z = 0$. This simple example immediately clarifies the versatility of our approach.

Table 2. In-plane components of the $\chi^{(3)}$ tensor for the non-magnetic and magnetic point groups of Classes 2 and 3. For the magnetic point groups, we highlight in red the elements that appear in the $\chi^{(3)}$ tensor only upon breaking of TRS.

Point group (unperturbed crystal)	Non-zero elements of the $\chi^{(3)}$ tensor	Allowed magnetic point group (crystal + light)	Non-zero elements of the $\chi^{(3)}$ tensor
622 6mm 6/mmm $\bar{6}m2$	<u>xxxx</u> =yyyy=xyyy+xyyx+xyxy	62'2' 6m'm' 6/mm'm' $\bar{6}m'2'$	<u>xxxx</u> =yyyy=xyyy+xyyx+xyxy <u>xxxy</u> =-yyyx=yyxy+yxyy+ <u>xyyy</u>
32 3m $\bar{3}m$	<u>xxxx</u> =yyyy=xyyy+xyyx+xyxy	32' 3m' $\bar{3}m'$	<u>xxxx</u> =yyyy=xyyy+xyyx+xyxy <u>xxxy</u> =-yyyx=yyxy+yxyy+ <u>xyyy</u>
422 4mm 4/mmm $\bar{4}2m$	<u>xxxx</u> =yyyy xyyy=yyxx xyxy=yxyx xyyx=yxxy	42'2' 4m'm' 4/mm'm' $\bar{4}2m'$	<u>xxxx</u> =yyyy xyyy=yyxx xyxy=yxyx xyyx=yxxy <u>xxxy</u> =-yyyx <u>xxyx</u> =-yyxy <u>xyxx</u> =-yxxy <u>yxxx</u> =- <u>xyyy</u>
222 mm2 mmm	<u>xxxx</u> ; yyyy; xxyy; xyxy; xyyx; yxyx; yxxy; yyxx	2'2'2 m'm'2 mm'2'* m'm'm	<u>xxxx</u> ; yyyy; xxyy; yyxx; xyxy; yxyx; xyyx; yxxy; <u>yxxx</u> ; xyyy; yxyy; yyxy; yyyx; xxyx; xyxx; xxxy
2 m 2/m	<u>xxxx</u> ; yyyy; xxyy; xyxy; xyxx; yxyx; yxxy; yyxx	2'* m'* 2'/m'*	<u>xxxx</u> ; yyyy; xxyy; yyxx; xyxy; yxyx; xyyx; yxxy; <u>yxxx</u> ; xyyy; yxyy; yyxy; yyyx; xxyx; xyxx; xxxy

* With respect to the notation of the Bilbao Crystallographic server [<https://www.cryst.ehu.es/>], where the C_2 rotational axis is oriented along the z axis, we made a transformation exchanging the y and z axes. This is made to account for light propagating perpendicular to the C_2 rotational axis, which is required for all-optical breaking of TRS.

** With respect to the notation of the Bilbao Crystallographic server [<https://www.cryst.ehu.es/>], where the mirror plane is the xy plane, we made a transformation exchanging the y and z axes. This is made to account for light propagating within the mirror plane, which is required for all-optical breaking of TRS.

S4 ELLIPTICAL THIRD-HARMONIC GENERATION – CLASSICAL/MACROSCOPIC DERIVATION BASED ON MAGNETIC POINT GROUPS

We start by comparing the $\chi^{(3)}$ elements of the magnetic point groups $\bar{6}m2$ and $\bar{3}m$ (mono- and bilayer TMD with preserved TRS), and $\bar{6}m'2'$ and $\bar{3}m'$ (mono- and bilayer TMD with broken TRS) [10, 11]. The non-zero in-plane elements of the nonlinear optical susceptibility tensor $\chi^{(3)}$ of the $\bar{6}m2$ and the $\bar{3}m$ point group are identical and given by:

$$\chi_{xxxx}^{(3)} = \chi_{yyyy}^{(3)} = 3\chi_{xxyy}^{(3)} = 3\chi_{xyyx}^{(3)} = 3\chi_{xyxy}^{(3)} \equiv \chi_{\text{int}}. \quad (1)$$

In addition to these, we find the following non-zero elements of $\chi^{(3)}$ for the $\bar{6}m'2'$ and $\bar{3}m'$ groups:

$$\chi_{xyyy}^{(3)} = 3\chi_{xxyy}^{(3)} = 3\chi_{xxyx}^{(3)} = 3\chi_{xyxx}^{(3)} = -3\chi_{yyyy}^{(3)} = -3\chi_{yyxy}^{(3)} = -3\chi_{yxyx}^{(3)} = -\chi_{yxxx}^{(3)} \equiv \chi_{\text{TRS}}, \quad (2)$$

where χ_{TRS} are the tensor elements that emerge from TRS breaking. The TH polarization for an arbitrary input is then given by:

$$\mathbf{P}^{(3)}(3\omega) = \varepsilon_0 \begin{pmatrix} \chi_{xxxx}^{(3)} & \chi_{xyyy}^{(3)} \\ \chi_{yxxx}^{(3)} & \chi_{yyyy}^{(3)} \end{pmatrix} \begin{pmatrix} \chi_{xxyy}^{(3)} + \chi_{xxyx}^{(3)} + \chi_{xyxy}^{(3)} \\ \chi_{yxyy}^{(3)} + \chi_{yyyx}^{(3)} + \chi_{yyxy}^{(3)} \end{pmatrix} \begin{pmatrix} \chi_{xxyy}^{(3)} + \chi_{xxyx}^{(3)} + \chi_{xyxy}^{(3)} \\ \chi_{yxyy}^{(3)} + \chi_{yyyx}^{(3)} + \chi_{yyxy}^{(3)} \end{pmatrix} \begin{pmatrix} E_x^3 \\ E_y^3 \\ E_x E_y^2 \\ E_x^2 E_y \end{pmatrix}, \quad (3)$$

where the blue elements are non-zero only in the $\bar{6}m'2'$ and $\bar{3}m'$ magnetic point groups (with broken TRS). We use the following expressions:

$$\begin{aligned} \chi_{xxyy}^{(3)} + \chi_{xxyx}^{(3)} + \chi_{xyxx}^{(3)} &= (\chi_{yxyy}^{(3)} + \chi_{yxyx}^{(3)} + \chi_{xyyy}^{(3)}) + \chi_{xxyx}^{(3)} + \chi_{xyxx}^{(3)} \\ &= (-\chi_{xxyx}^{(3)} - \chi_{xyxx}^{(3)} - \chi_{yxxx}^{(3)}) + \chi_{xxyx}^{(3)} + \chi_{xyxx}^{(3)} \\ &= -\chi_{yxxx}^{(3)} \\ &= \chi_{xyyy}^{(3)} = \chi_{\text{TRS}} \end{aligned} \quad (4)$$

and

$$\begin{aligned}
\chi_{yxyy}^{(3)} + \chi_{yyyx}^{(3)} + \chi_{yyxy}^{(3)} &= \chi_{yxyy}^{(3)} - (\chi_{yyxy}^{(3)} + \chi_{yxyy}^{(3)} + \chi_{xyyy}^{(3)}) + \chi_{yyxy}^{(3)} \\
&= \chi_{yxyy}^{(3)} - \chi_{yyxy}^{(3)} - \chi_{yxyy}^{(3)} - \chi_{xyyy}^{(3)} + \chi_{yyxy}^{(3)} \\
&= -\chi_{xyyy}^{(3)} = \chi_{\text{TRS}}
\end{aligned} \tag{5}$$

as well as

$$\chi_{xxyy}^{(3)} + \chi_{xyyx}^{(3)} + \chi_{xyxy}^{(3)} = \chi_{xxxx}^{(3)} = \chi_{yyyy}^{(3)} = \chi_{\text{int}} \tag{6}$$

$$\chi_{xxyy}^{(3)} = \chi_{yyxx}^{(3)} \tag{7}$$

$$\chi_{xyyx}^{(3)} = \chi_{yxyx}^{(3)} \tag{8}$$

$$\chi_{xyxy}^{(3)} = \chi_{yxxy}^{(3)}. \tag{9}$$

We can rewrite the TH polarization:

$$\begin{aligned}
\mathbf{P}^{(3)}(3\omega) &= \varepsilon_0 \begin{pmatrix} \chi_{\text{int}} & \chi_{\text{TRS}} & \chi_{\text{int}} & \chi_{\text{TRS}} \\ -\chi_{\text{TRS}} & \chi_{\text{int}} & -\chi_{\text{TRS}} & \chi_{\text{int}} \end{pmatrix} \begin{pmatrix} E_x^3 \\ E_y^3 \\ E_x E_y^2 \\ E_x^2 E_y \end{pmatrix} \\
&= \varepsilon_0 \begin{pmatrix} \chi_{\text{int}}(E_x^3 + E_x E_y^2) + \chi_{\text{TRS}}(E_y^3 + E_x^2 E_y) \\ \chi_{\text{int}}(E_y^3 + E_x^2 E_y) - \chi_{\text{TRS}}(E_x^3 + E_x E_y^2) \end{pmatrix}.
\end{aligned} \tag{10}$$

The electromagnetic field in the case of elliptical polarization can be written as:

$$\mathbf{E} = E \exp\left\{i\frac{\pi}{4}\right\} \begin{pmatrix} 1 & 0 \\ 0 & -i \end{pmatrix} \cdot \begin{pmatrix} \cos(\alpha) \\ \sin(\alpha) \end{pmatrix} = E \exp\left\{i\frac{\pi}{4}\right\} \begin{pmatrix} \cos(\alpha) \\ -i \sin(\alpha) \end{pmatrix}, \tag{11}$$

where E is the amplitude of the driving field and α the rotation angle of the polarization plane with respect to the plane of incidence. The phase factor $\exp\{i\frac{\pi}{4}\}$ can be neglected, since it is a constant phase offset [12]. By using equation (11), we can write equation (10) as:

$$\begin{aligned}
\mathbf{P}^{(3)}(3\omega) &= \varepsilon_0 E^3 \begin{pmatrix} \chi_{\text{int}}(\cos(\alpha) \cos(2\alpha)) - i\chi_{\text{TRS}}(\sin(\alpha) \cos(2\alpha)) \\ -i\chi_{\text{int}}(\sin(\alpha) \cos(2\alpha)) - \chi_{\text{TRS}}(\cos(\alpha) \cos(2\alpha)) \end{pmatrix} \\
&= \varepsilon_0 E^3 \cos(2\alpha) \begin{pmatrix} \chi_{\text{int}} \cos(\alpha) - i\chi_{\text{TRS}} \sin(\alpha) \\ -i\chi_{\text{int}} \sin(\alpha) - \chi_{\text{TRS}} \cos(\alpha) \end{pmatrix}.
\end{aligned} \tag{12}$$

For $\alpha = \pm \frac{\pi}{4}$ (circularly polarized light), we obtain $\mathbf{P}^{(3)}(3\omega) = 0$ regardless of the values of χ_{int} and χ_{TRS} , as expected from the conservation of angular momentum for THG in crystals with 3-fold rotational symmetry [13]. In other words, circular TH output is forbidden in our system. For all other cases, we obtain an elliptically polarized TH output from an elliptically polarized input. Next, we want to derive an expression for the rotation angle θ of the TH polarization output relative to the input. The angle θ is related to the Stokes parameters S_1 and S_2 as

$$S_1 = I_p \cos(2\theta) \cos(2\Psi), \tag{13}$$

$$S_2 = I_p \cos(2\theta) \sin(2\Psi), \tag{14}$$

where I_p , 2θ and 2Ψ are the spherical coordinates of the polarization state on the Poincaré sphere. This results in an expression for the rotation angle θ of TH elliptical polarization as:

$$\tan 2\theta = \frac{S_2}{S_1}. \tag{15}$$

The complex NLO susceptibilities with their real and imaginary parts can be written in the general case as $\chi_{\text{int}} := a + i\tilde{a}$ and $\chi_{\text{TRS}} := b + i\tilde{b}$, where a and b are the real part and \tilde{a} and \tilde{b} the imaginary part. Using this substitution, we obtain for the TH polarization:

$$\mathbf{P}^{(3)}(3\omega) = \varepsilon_0 E^3 \cos(2\alpha) \begin{pmatrix} (a + i\tilde{a}) \cos(\alpha) - i(b + i\tilde{b}) \sin(\alpha) \\ -i(a + i\tilde{a}) \sin(\alpha) - (b + i\tilde{b}) \cos(\alpha) \end{pmatrix}, \tag{16}$$

where we define

$$\mathbf{P}^{(3)}(3\omega) := \cos(2\alpha) \left[\begin{pmatrix} p_x \\ p_y \end{pmatrix} + i \begin{pmatrix} q_x \\ q_y \end{pmatrix} \right] \tag{17}$$

as a general expression of the polarization $\mathbf{P}^{(3)}(3\omega)$ with $P_x = p_x + iq_x$ and $P_y = p_y + iq_y$. Accordingly, p_x , p_y , q_x and q_y are given as:

$$p_x = a \cos(\alpha) + \tilde{b} \sin(\alpha) \quad (18)$$

$$p_y = \tilde{a} \sin(\alpha) - b \cos(\alpha) \quad (19)$$

$$q_x = \tilde{a} \cos(\alpha) - b \sin(\alpha) \quad (20)$$

$$q_y = - \left(a \sin(\alpha) + \tilde{b} \cos(\alpha) \right) . \quad (21)$$

The Stokes parameter S_1 can be expressed as

$$\begin{aligned} S_1 &\propto |P_x|^2 - |P_y|^2 \\ &= p_x^2 + q_x^2 - p_y^2 - q_y^2 \\ &\propto \cos^2(2\alpha) \left[(a^2 + \tilde{a}^2 - b^2 - \tilde{b}^2) \cos^2(\alpha) + (\tilde{b}^2 + b^2 - \tilde{a}^2 - a^2) \sin^2(\alpha) \right] \\ &= \cos^3(2\alpha) (|\chi_{\text{int}}|^2 - |\chi_{\text{TRS}}|^2) \end{aligned} \quad (22)$$

and

$$S_2 \propto 2 (p_x p_y + q_x q_y) \propto -2 \cos^3(2\alpha) (ab + \tilde{a}\tilde{b}) . \quad (23)$$

Using equation (15) we obtain a rotation angle of the TH elliptical polarization θ of

$$\tan 2\theta = \frac{-2 \cos^3(2\alpha) (ab + \tilde{a}\tilde{b})}{\cos^3(2\alpha) (|\chi_{\text{int}}|^2 - |\chi_{\text{TRS}}|^2)} \quad (24)$$

which can be simplified to the same expression of elliptical SHG presented in Ref. [14]:

$$\tan 2\theta \approx -2 \frac{ab + \tilde{a}\tilde{b}}{|\chi_{\text{int}}|^2} \approx -2 \frac{\text{Im}(\chi_{\text{TRS}})}{\text{Im}(\chi_{\text{int}})} \quad (25)$$

under the assumption that the effect of the TRS breaking on the NLO susceptibility is small compared to the intrinsic NLO susceptibility $|\chi_{\text{int}}| \gg |\chi_{\text{TRS}}|$ and considering that the NLO susceptibility is purely imaginary ($\text{Re}(\chi_{\text{int}}) = \text{Re}(\chi_{\text{TRS}}) = 0$) at optical resonances.

S5 OPTICAL STARK AND BLOCH-SIEGERT SHIFTS WITH ELLIPTICAL POLARIZATION

An off-resonant electromagnetic field radiating on a material induces an energy shift that can be obtained from time-dependent perturbation theory. Here, we follow the semi-classical derivation used in Ref. [15]. We express the incoming elliptically polarized light (11) of ellipticity angle α and frequency ω in the time domain as

$$\boldsymbol{\mathcal{E}}(t) = \mathcal{E} \begin{pmatrix} \cos \alpha \cos \omega t \\ \sin \alpha \sin \omega t \end{pmatrix} = \frac{\mathcal{E}}{2} \left[e^{i\omega t} \begin{pmatrix} \cos \alpha \\ -i \sin \alpha \end{pmatrix} + e^{-i\omega t} \begin{pmatrix} \cos \alpha \\ i \sin \alpha \end{pmatrix} \right]. \quad (26)$$

The perturbation Hamiltonian that is induced by $\boldsymbol{\mathcal{E}}$ is [15],

$$\begin{aligned} H_{vc}(t) &= \mathbf{d}_{cv}(\tau) \cdot \boldsymbol{\mathcal{E}}(t) \\ &= \frac{\mathcal{E}}{2} [e^{i\omega t} (d_{cv}^x(\tau) \cos \alpha - i d_{cv}^y(\tau) \sin \alpha) + e^{-i\omega t} (d_{cv}^x(\tau) \cos \alpha + i d_{cv}^y(\tau) \sin \alpha)] \\ &= \frac{\mathcal{E} d_0}{2} [e^{i\omega t} (\cos \alpha + \tau \sin \alpha) + e^{-i\omega t} (\cos \alpha - \tau \sin \alpha)]. \end{aligned} \quad (27)$$

Here, $d_{cv}^x(\tau) = d_0$ and $d_{cv}^y(\tau) = i\tau d_0$ are the dipole matrix elements [16] between the valence band maximum and the conduction band minimum at the $\pm K$ points of a monolayer TMD, $\pm K = \frac{2\pi}{3}(\sqrt{3}, \tau)$, where $\tau = \pm 1$.

The induced energy shift of the valence band can be obtained through the standard time-dependent perturbation theory as done in [15],

$$\begin{aligned} \Delta E_v(t) &= H_{vc}^*(t) e^{-i\omega_0 t} \frac{1}{i\hbar} \int_0^t H_{vc}(t') e^{i\omega_0 t'} dt' \\ &= \frac{\mathcal{E} d_0^*}{2i\hbar} [e^{i\omega t} (\cos \alpha - \tau \sin \alpha) + e^{-i\omega t} (\cos \alpha + \tau \sin \alpha)] e^{-i\omega_0 t} \\ &\quad \int_0^t \frac{\mathcal{E} d_0}{2} [e^{i\omega t'} (\cos \alpha + \tau \sin \alpha) + e^{-i\omega t'} (\cos \alpha - \tau \sin \alpha)] e^{i\omega_0 t'} dt' \\ &= \frac{\mathcal{E}^2 |d_0|^2}{4i\hbar} [e^{-i(\omega_0 - \omega)t} (\cos \alpha - \tau \sin \alpha) + e^{-i(\omega_0 + \omega)t} (\cos \alpha + \tau \sin \alpha)] \\ &\quad \left[\left(\frac{e^{i(\omega_0 + \omega)t} - 1}{i(\omega_0 + \omega)} \right) (\cos \alpha + \tau \sin \alpha) + \left(\frac{e^{i(\omega_0 - \omega)t} - 1}{i(\omega_0 - \omega)} \right) (\cos \alpha - \tau \sin \alpha) \right] \\ &= \frac{\mathcal{E}^2 |d_0|^2}{4i\hbar} \left[\left(\frac{e^{2i\omega t} - e^{-i(\omega_0 - \omega)t}}{i(\omega_0 + \omega)} + \frac{e^{-2i\omega t} - e^{-i(\omega_0 + \omega)t}}{i(\omega_0 - \omega)} \right) (\cos^2 \alpha - \sin^2 \alpha) \right. \\ &\quad \left. + \left(\frac{1 - e^{-i(\omega_0 - \omega)t}}{i(\omega_0 - \omega)} \right) (1 - 2\tau \sin \alpha \cos \alpha) + \left(\frac{1 - e^{-i(\omega_0 + \omega)t}}{i(\omega_0 + \omega)} \right) (1 + 2\tau \sin \alpha \cos \alpha) \right], \end{aligned} \quad (28)$$

where $\omega_0 = \varepsilon_{cv}/\hbar$ is the frequency associated with the bandgap ε_{cv} at $\pm K$. The energy shift $\Delta E_v(t)$ saturates at its mean value, which can be obtained by averaging over time,

$$\overline{\Delta E_v} = \lim_{T \rightarrow \infty} \frac{1}{T} \int_0^T \Delta E_v(t) dt = -\frac{\mathcal{E}^2 |d_0|^2}{4} \left(\frac{1 + \tau \sin 2\alpha}{\varepsilon_{cv} + \hbar\omega} + \frac{1 - \tau \sin 2\alpha}{\varepsilon_{cv} - \hbar\omega} \right) =: -\Delta E_{\tau, \alpha}. \quad (29)$$

For the conduction band, the energy is the same but with an opposite sign,

$$\overline{\Delta E_c} = -\overline{\Delta E_v} = \Delta E_{\tau, \alpha}, \quad (30)$$

The gap opening $2\Delta E_{\tau, \alpha}$ for a monolayer TMD depends on the valley index τ and thus is responsible for breaking the TRS. For further simplification, we employ the absolute value of the dipole moment $d = \sqrt{|d_{cv}^x|^2 + |d_{cv}^y|^2} = \sqrt{2}|d_0|$ which leads to

$$\Delta E_{\tau, \alpha} = \frac{\mathcal{E}^2 d^2}{8} \left(\frac{1 + \tau \sin 2\alpha}{\varepsilon_{cv} + \hbar\omega} + \frac{1 - \tau \sin 2\alpha}{\varepsilon_{cv} - \hbar\omega} \right). \quad (31)$$

Since we are studying THG, we can use $\hbar\omega = \varepsilon_{cv}/3$ which simplifies the above equation into

$$\Delta E_{\tau, \alpha} = \frac{3\mathcal{E}^2 d^2}{32\varepsilon_{cv}} (3 - \tau \sin 2\alpha). \quad (32)$$

For bilayer TMDs, the OS and BS effects can similarly be calculated using [17, equation (5)]

$$\Delta E_a = -\frac{\mathcal{E}^2}{4} \sum_b \left(\frac{|\langle b | \mathbf{u} \cdot \mathbf{d} | a \rangle|^2}{\varepsilon_b - \varepsilon_a - \hbar\omega} + \frac{|\langle a | \mathbf{u} \cdot \mathbf{d} | b \rangle|^2}{\varepsilon_b - \varepsilon_a + \hbar\omega} \right), \quad (33)$$

where, $\mathbf{u} = \cos \alpha \hat{x} - i \sin \alpha \hat{y}$, and, a and b are energy states. Therefore,

$$\overline{\Delta E_{c, \tau, \mathcal{L}, \sigma}} = -\overline{\Delta E_{v, \tau, \mathcal{L}, \sigma}} = \frac{\mathcal{E}^2}{4} \left(\frac{|\cos \alpha d_{cv}^x - i \sin \alpha d_{cv}^y|^2}{\varepsilon_{cv} + \hbar\omega} + \frac{|\cos \alpha d_{cv}^x + i \sin \alpha d_{cv}^y|^2}{\varepsilon_{cv} - \hbar\omega} \right) = \Delta E_{\sigma, \alpha}, \quad (34)$$

where $\mathcal{L} = 'u', 'l'$ indicates 'upper' and 'lower' layer respectively, $\sigma = \uparrow, \downarrow$ (or ± 1) indicates the spin. We use equation (72), to evaluate the energy shift $\Delta E_{\sigma, \alpha}$ for the bilayer,

$$\Delta E_{\sigma, \alpha} = \frac{3\mathcal{E}^2 d_{\text{BL}}^2}{32\varepsilon_{cv}} (3 + \sigma \sin 2\alpha). \quad (35)$$

We see that the energy shift for the bilayer depends on the spin σ . For the monolayer, equation (32), we omit the spin because every valley has a predefined spin (spin-valley locking). From equation (72), we evaluate for the bilayer,

$$\begin{aligned} \Delta E_{C_{\uparrow}^u}^K &= -\Delta E_{V_{\uparrow}^u}^K = \Delta E_{C_{\uparrow}^l}^{-K} = -\Delta E_{V_{\uparrow}^l}^{-K} = \frac{3\mathcal{E}^2 d_{\text{BL}}^2}{32\varepsilon_{cv}} (3 + \sin 2\alpha), \\ \Delta E_{C_{\downarrow}^l}^K &= -\Delta E_{V_{\downarrow}^l}^K = \Delta E_{C_{\downarrow}^u}^{-K} = -\Delta E_{V_{\downarrow}^u}^{-K} = \frac{3\mathcal{E}^2 d_{\text{BL}}^2}{32\varepsilon_{cv}} (3 - \sin 2\alpha), \end{aligned} \quad (36)$$

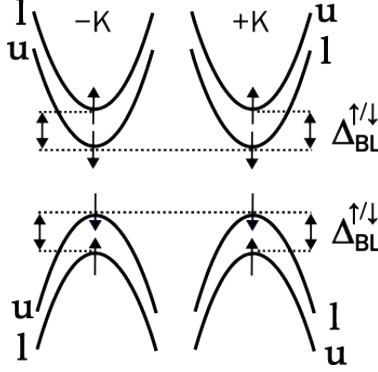


Fig. S3: TRS breaking in bilayer TMDs. Here we only include the states with a bandgap that is resonant with the TH photon energy.

where we have employed the dipole $d_{\text{BL}} = aq|\gamma|/\epsilon_{cv}$ emerging in the bilayer (BL). We see from equation (36) that the OS and BS effects are higher for Spin-up states than for spin down states as seen in figure S3. Here, $\Delta_{\text{BL}}^{\uparrow/\downarrow}$ is the energy difference between the spin up and spin down states in each valley

$$\Delta_{\text{BL}}^{\uparrow/\downarrow} := \frac{3\mathcal{E}^2 d_{\text{BL}}^2}{16\epsilon_{cv}} \sin 2\alpha. \quad (37)$$

S6 QUANTUM-MECHANICAL MODEL FOR THIRD-HARMONIC GENERATION

General analytical expression for the $\chi^{(3)}$ tensor of a solid

In this section, we focus on analytical expressions for the elements of the third-order susceptibility, $\chi_{dcb a}^{(3)}(-\omega_3; \omega_\gamma, \omega_\beta, \omega_\alpha)$ with $d, c, b, a \in \{x, y\}$ where $\omega_\alpha, \omega_\beta$, and ω_γ are the incoming frequencies and $\omega_3 = \omega_\alpha + \omega_\beta + \omega_\gamma$ is the frequency of the outgoing four-wave mixing signal. A general analytical expression for the third order optical susceptibility has

been derived in Ref. [18, equation (35)]:

$$\begin{aligned}
\frac{\chi_{dcba}^{(3)}}{C} = & \sum_{l,m,n,p,\mathbf{k}} \frac{r_{mn}^d}{\varepsilon_{nm} - \omega_3} \left[\frac{r_{nl}^c}{\varepsilon_{lm} - \omega_2} \left(\frac{r_{lp}^b r_{pm}^a f_{mp}}{\varepsilon_{pm} - \omega_1} - \frac{r_{lp}^a r_{pm}^b f_{pl}}{\varepsilon_{lp} - \omega_1} \right) - \left(\frac{r_{nl}^b r_{lp}^a f_{pl}}{\varepsilon_{lp} - \omega_1} - \frac{r_{nl}^a r_{lp}^b f_{ln}}{\varepsilon_{nl} - \omega_1} \right) \frac{r_{pm}^c}{\varepsilon_{np} - \omega_2} \right] \\
& + i \sum_{l,m,n,\mathbf{k}} \frac{r_{mn}^d}{\varepsilon_{nm} - \omega_3} \left[\frac{1}{\varepsilon_{nm} - \omega_2} \left(\frac{r_{nl}^b r_{lm}^a f_{ml}}{\varepsilon_{lm} - \omega_1} - \frac{r_{nl}^a r_{lm}^b f_{ln}}{\varepsilon_{nl} - \omega_1} \right) \right]_{;kc} \\
& + i \sum_{l,m,n,\mathbf{k}} \frac{r_{mn}^d}{\varepsilon_{nm} - \omega_3} \left[\frac{r_{nl}^c}{\varepsilon_{lm} - \omega_2} \left(\frac{r_{lm}^a f_{ml}}{\varepsilon_{lm} - \omega_1} \right)_{;kb} - \left(\frac{r_{nl}^a f_{ln}}{\varepsilon_{nl} - \omega_1} \right)_{;kb} \frac{r_{lm}^c}{\varepsilon_{nl} - \omega_2} \right] \\
& - \sum_{m,n,\mathbf{k}} \frac{r_{mn}^d}{\varepsilon_{nm} - \omega_3} \left[\frac{1}{\varepsilon_{nm} - \omega_2} \left(\frac{r_{nm}^a f_{mn}}{\varepsilon_{nm} - \omega_1} \right)_{;kb} \right]_{;kc}. \tag{38}
\end{aligned}$$

Here, ε_{nm} is the difference between the energies of the bands n and m at crystal momentum \mathbf{k} , $\omega_1 = \omega_\alpha$, $\omega_2 = \omega_\alpha + \omega_\beta$, $\mathbf{r}_{nm} = (1 - \delta_{nm})\mathbf{d}_{nm}$, where \mathbf{d}_{nm} is the dipole matrix element which can be computed as integral over the Brillouin zone volume Ω using the lattice-periodic functions $u_{n\mathbf{k}}(\mathbf{r})$,

$$\mathbf{d}_{nm} = \frac{(2\pi)^3 i}{\Omega} \int_{\Omega} d^3\mathbf{r} u_{n\mathbf{k}}^*(\mathbf{r}) \nabla_{\mathbf{k}} u_{m\mathbf{k}}(\mathbf{r}). \tag{39}$$

In equation (38), the generalized derivative $(S_{nm})_{;\mathbf{k}} \equiv \frac{\partial S_{nm}}{\partial \mathbf{k}} - iS_{nm}(\mathbf{d}_{nn} - \mathbf{d}_{mm})$ of a general quantity S is used. We have suppressed all \mathbf{k} -dependencies in equation (38).

Model Hamiltonian for monolayer TMDs

We employ a two-band model applicable near the $\pm K$ points of the Brillouin zone to represent the TMD Hamiltonian [16, 19],

$$\mathbf{h}(\mathbf{k}) = \begin{pmatrix} \Delta + \mathbf{\Delta} E_{\tau,\alpha} & \gamma^* f^*(\mathbf{k}) \\ \gamma f(\mathbf{k}) & -\Delta - \mathbf{\Delta} E_{\tau,\alpha} \end{pmatrix}, \tag{40}$$

where Δ is the on-site energy, γ is an effective hopping, and

$$f(\mathbf{k}) = \frac{2}{\sqrt{3}} e^{-i\frac{\pi}{3}} \left(e^{ik_x a/\sqrt{3}} + 2e^{-ik_x a/(2\sqrt{3})} \cos(k_y a/2) \right) \tag{41}$$

with lattice constant a . The term $\mathbf{\Delta} E_{\tau,\alpha}$ is the TRS breaking term due to the OS and BS effects at the $\pm K = \frac{2\pi}{3}(\sqrt{3}, \tau)$ points, where $\tau = \pm 1$ (see S4). As our driving pulses excite the TH resonantly at the $\pm K$ points, we employ the Taylor expansion of $f(\mathbf{k})$ near $\pm K$,

$$f(\mathbf{k}) = -(i\kappa_x + \kappa_y \tau) + \zeta_2(\kappa_x + i\kappa_y \tau)^2 + \zeta_3(i\kappa_x + \kappa_y \tau)(\kappa_x^2 + \kappa_y^2) + \mathcal{O}(\kappa^4) \tag{42}$$

with $\kappa_{x(y)} = a(k_{x(y)} - K_{x(y)})$, $\zeta_2 = \frac{\sqrt{3}}{12}$, $\zeta_3 = \frac{1}{24}$.

Evaluating $\chi^{(3)}$ for a monolayer TMD

For THG, *i.e.* , $\omega_\gamma = \omega_\beta = \omega_\alpha =: \omega$, a two band model with occupied valence band ($f_v = 1$) and empty conduction band ($f_c = 0$), equation (38) simplifies to

$$\frac{\chi_{dcba}^{(3)}}{C} = \mathcal{P}_I \sum_{\mathbf{k}} \frac{-d_{vc}^d(\mathbf{k})d_{cv}^c(\mathbf{k})}{(\varepsilon_{cv}(\mathbf{k}) - 3\hbar\omega + i\hbar/T_2)\hbar\omega} \left(\frac{d_{cv}^a(\mathbf{k})d_{vc}^b(\mathbf{k})}{\varepsilon_{cv}(\mathbf{k}) - \hbar\omega} + \frac{d_{vc}^a(\mathbf{k})d_{cv}^b(\mathbf{k})}{\varepsilon_{vc}(\mathbf{k}) - \hbar\omega} \right) - \frac{d_{vc}^d(\mathbf{k})}{\varepsilon_{cv}(\mathbf{k}) - 3\omega + i\hbar/T_2} \frac{\partial}{\partial k_c} \left[\frac{1}{\varepsilon_{cv}(\mathbf{k}) - 2\omega} \frac{\partial}{\partial k_b} \left(\frac{d_{cv}^a(\mathbf{k})f_{vc}}{\varepsilon_{cv}(\mathbf{k}) - \omega} \right) \right]. \quad (43)$$

Here, we have included the dephasing rate $1/T_2$ [16, 20] as it is commonly used to model ultrafast decoherence processes which include electron-phonon and electron-electron scattering. The symbol \mathcal{P}_I denotes the intrinsic permutation operator, since c, b, a are dummy indexes which can be freely exchanged in the case of THG. We have excluded terms with \mathbf{d}_{vv} and \mathbf{d}_{cc} from equation (43) since they are quadratic in \mathbf{k} for the model Hamiltonian (equation (40)) [16].

For TH resonant driving, $\varepsilon_{cv} \approx 3\hbar\omega$ in equation (43) at the $\pm K$ points, $\varepsilon_{cv}(\pm K) = 2(\Delta + \Delta E_{\tau,\alpha})$, the effect of TRS breaking *via* $\Delta E_{\tau,\alpha}$ is dominant in the term

$$\frac{1}{\varepsilon_{cv}(\pm K) + i\hbar/T_2 - 3\hbar\omega} = \frac{1}{2(\Delta + \Delta E_{\tau,\alpha}) + i\hbar/T_2 - 3\hbar\omega}. \quad (44)$$

For evaluating equation (43) besides the resonant term (44), we calculate the dipoles and the eigenstates of the unperturbed Hamiltonian ($\Delta E_{\tau,\alpha} = 0$). The eigenvalues close to $\pm K$ are

$$\varepsilon_v = -\sqrt{\Delta^2 + |\gamma f|^2} \stackrel{\text{at } \pm K}{=} -\Delta, \quad \varepsilon_c = \sqrt{\Delta^2 + |\gamma f|^2} \stackrel{\text{at } \pm K}{=} \Delta, \quad \varepsilon_{cv} \stackrel{\text{at } \pm K}{=} 2\Delta. \quad (45)$$

and the eigenstates are

$$|v\mathbf{k}\rangle = \frac{1}{N(\mathbf{k})} \begin{pmatrix} -\gamma^* f^*(\mathbf{k}) \\ \Delta + \sqrt{\Delta^2 + |\gamma f(\mathbf{k})|^2} \end{pmatrix}, \quad |c\mathbf{k}\rangle = \frac{1}{N(\mathbf{k})} \begin{pmatrix} \Delta + \sqrt{\Delta^2 + |\gamma f(\mathbf{k})|^2} \\ \gamma f(\mathbf{k}) \end{pmatrix}, \quad (46)$$

where

$$N(\mathbf{k}) = \sqrt{\left(\Delta + \sqrt{\Delta^2 + |\gamma f(\mathbf{k})|^2} \right)^2 + |\gamma f|^2} \stackrel{\text{at } \pm K}{=} 2\Delta. \quad (47)$$

Therefore,

$$|v\mathbf{k}\rangle = \begin{pmatrix} -\frac{\gamma^* f^*(\mathbf{k})}{2\Delta} \\ 1 \end{pmatrix}, \quad |c\mathbf{k}\rangle = \begin{pmatrix} 1 \\ \frac{\gamma f(\mathbf{k})}{2\Delta} \end{pmatrix}. \quad (48)$$

Thus, the dipole matrix elements are

$$\begin{aligned}
d_{cv}^x &= iq \langle c\mathbf{k} | \frac{\partial}{\partial k_x} | v\mathbf{k} \rangle = \frac{aq\gamma^*}{2\Delta} f_x^*(\mathbf{k}), \\
d_{cv}^y &= iq \langle c\mathbf{k} | \frac{\partial}{\partial k_y} | v\mathbf{k} \rangle = \frac{aq\gamma^*}{2\Delta} f_y^*(\mathbf{k}), \\
d_{vc}^x &= iq \langle v\mathbf{k} | \frac{\partial}{\partial k_x} | c\mathbf{k} \rangle = \frac{aq\gamma}{2\Delta} f_x(\mathbf{k}), \\
d_{vc}^y &= iq \langle v\mathbf{k} | \frac{\partial}{\partial k_y} | c\mathbf{k} \rangle = \frac{aq\gamma}{2\Delta} f_y(\mathbf{k}),
\end{aligned} \tag{49}$$

where q is the charge of an electron and,

$$\begin{aligned}
f_x(\mathbf{k}) &= 1 + 2i\zeta_2\kappa_x - 2\zeta_2\tau\kappa_y - 3\zeta_3\kappa_x^2 + 2i\zeta_3\tau\kappa_x\kappa_y - \zeta_3\kappa_y^2 + \mathcal{O}(\kappa^3), \\
f_y(\mathbf{k}) &= -i\tau - 2\zeta_2\tau\kappa_x - 2i\zeta_2\kappa_y + i\zeta_3\tau\kappa_x^2 - 2\zeta_3\kappa_x\kappa_y + 3i\zeta_3\tau\kappa_y^2 + \mathcal{O}(\kappa^3).
\end{aligned} \tag{50}$$

We evaluate $\chi_{dcba}^{(3)}$ from equation (43) at the resonant $\pm K$ points using the band energies (45), the dipoles (49) and the TH resonance (44),

$$\chi_{xxxx}^{(3)} = \sum_{\tau=\pm 1} \chi_{xxxx}^{(3)}(\tau) = \sum_{\tau=\pm 1} \frac{\mathcal{C}}{2(\Delta + \Delta E_{\tau,\alpha}) - 3\hbar\omega + i\hbar/T_2} = \frac{2\Delta_\omega}{\Delta_\omega^2 - (\Delta_{\text{gap}}^{\pm K})^2} \mathcal{C} = \chi_{\text{int}} \tag{51}$$

with

$$\Delta_\omega := 2\Delta - 3\hbar\omega + \frac{i\hbar}{T_2} + \sum_{\tau=\pm 1} \Delta E_{\tau,\alpha} \stackrel{(32)}{=} 2\Delta - 3\hbar\omega + \frac{i\hbar}{T_2} + \frac{9\mathcal{E}^2 d^2}{32\Delta}, \tag{52}$$

$$\Delta_{\text{gap}}^{\pm K} := \sum_{\tau=\pm 1} (-\tau) \cdot \Delta E_{\tau,\alpha} = \Delta E_{-K,\alpha} - \Delta E_{+K,\alpha} \stackrel{(32)}{=} \frac{3\mathcal{E}^2 d^2}{32\Delta} \sin 2\alpha, \tag{53}$$

$$\mathcal{C} := C \frac{a^4 q^4 |\gamma|^2 (|\gamma|^2 (2\Delta^2 + 5\Delta\hbar\omega - \hbar\omega^2) + 6\Delta^2 \zeta_3 (4\Delta^2 - \hbar\omega^2))}{4\Delta^4 (\Delta - \hbar\omega) (2\Delta - \hbar\omega)^2 (2\Delta + \hbar\omega)}. \tag{54}$$

Similarly, the expression for $\chi_{xyyy}^{(3)}$ reads

$$\chi_{xyyy}^{(3)} = \sum_{\tau=\pm 1} \chi_{xyyy}^{(3)}(\tau) = \sum_{\tau=\pm 1} \frac{i\tau \mathcal{C}}{2(\Delta + \Delta E_{\tau,\alpha}) - 3\hbar\omega + i\hbar/T_2} = \frac{2i\Delta_{\text{gap}}^{\pm K}}{\Delta_\omega^2 - (\Delta_{\text{gap}}^{\pm K})^2} \mathcal{C} = \chi_{\text{TRS}}. \tag{55}$$

Moreover, it is possible by evaluating equation (43) to validate that the relations for the $\bar{6}m'2'$ magnetic point group are fulfilled (detailed calculation not shown):

$$\begin{aligned}
\chi_{xxxx}^{(3)} &= \chi_{yyyy}^{(3)} = 3\chi_{xxyy}^{(3)} = 3\chi_{xyyx}^{(3)} = 3\chi_{xyxy}^{(3)} \equiv \chi_{\text{int}} \\
\chi_{xyyy}^{(3)} &= 3\chi_{xxyy}^{(3)} = 3\chi_{xxyx}^{(3)} = 3\chi_{xyxx}^{(3)} = -3\chi_{xyyy}^{(3)} = -3\chi_{yyxy}^{(3)} = -3\chi_{yxyx}^{(3)} = -\chi_{yxxx}^{(3)} \equiv \chi_{\text{TRS}}.
\end{aligned}$$

Evaluation of the third-harmonic rotation from the $\chi^{(3)}$ tensor

For evaluating the polarization rotation of the TH, we start from the third-order polarization,

$$P_d = \varepsilon_0 \sum_{a,b,c} \chi_{dcba}^{(3)} E_c E_b E_a \quad (56)$$

$$= \varepsilon_0 \left[\chi_{dxxx}^{(3)} E_x^3 + (\chi_{dxdy}^{(3)} + \chi_{dxyx}^{(3)} + \chi_{dyxx}^{(3)}) E_x^2 E_y + (\chi_{dxyy}^{(3)} + \chi_{dyyx}^{(3)} + \chi_{dyxy}^{(3)}) E_x E_y^2 + \chi_{dyyy}^{(3)} E_y^3 \right]. \quad (57)$$

Focusing on the x-component of the emission ($d = x$), we know from the symmetry of the $\bar{6}m'2'$ magnetic point group that

$$\chi_{xxxy}^{(3)} + \chi_{xxyx}^{(3)} + \chi_{xyxx}^{(3)} = \chi_{xyyy}^{(3)} \quad \text{and} \quad \chi_{xxyy}^{(3)} + \chi_{xyyx}^{(3)} + \chi_{xyxy}^{(3)} = \chi_{xxxx}^{(3)}.$$

As driving field, we employ equation (11) without the phase factor $\exp\{i\frac{\pi}{4}\}$,

$$\mathbf{E}_{\text{IN}} = \begin{pmatrix} E_x \\ E_y \end{pmatrix} = \mathcal{E} \begin{pmatrix} \cos \alpha \\ i \sin \alpha \end{pmatrix}. \quad (58)$$

With this, equation (57) for emission along the x direction ($d = x$) becomes

$$\begin{aligned} P_x &= \varepsilon_0 (\chi_{xxxx}^{(3)} E_x^3 + \chi_{xyyy}^{(3)} E_x^2 E_y + \chi_{xxxx}^{(3)} E_x E_y^2 + \chi_{xyyy}^{(3)} E_y^3) \\ &= \varepsilon_0 \chi_{xxxx}^{(3)} E_x (E_x^2 + E_y^2) + \varepsilon_0 \chi_{xyyy}^{(3)} E_y (E_x^2 + E_y^2) \\ &= \varepsilon_0 (E_x^2 + E_y^2) (\chi_{\text{int}} E_x + \chi_{\text{TRS}} E_y) \\ &\stackrel{(58)}{=} \varepsilon_0 \mathcal{E}^3 (\cos^2 \alpha - \sin^2 \alpha) (\chi_{\text{int}} \cos \alpha + i \chi_{\text{TRS}} \sin \alpha) \\ &= \varepsilon_0 \mathcal{E}^3 \cos 2\alpha (\chi_{\text{int}} \cos \alpha + i \chi_{\text{TRS}} \sin \alpha). \end{aligned} \quad (59)$$

Similarly,

$$\begin{aligned} P_y &= \varepsilon_0 (\chi_{yyyy}^{(3)} E_y^3 + \chi_{yxxx}^{(3)} E_y^2 E_x + \chi_{yyyy}^{(3)} E_y E_x^2 + \chi_{yxxx}^{(3)} E_x^3) \\ &= \varepsilon_0 \chi_{yyyy}^{(3)} E_y (E_x^2 + E_y^2) + \varepsilon_0 \chi_{yxxx}^{(3)} E_x (E_x^2 + E_y^2) \\ &= \varepsilon_0 (E_x^2 + E_y^2) (\chi_{yxxx}^{(3)} E_x + \chi_{yyyy}^{(3)} E_y) \\ &\stackrel{(58)}{=} \varepsilon_0 \mathcal{E}^3 (\cos^2 \alpha - \sin^2 \alpha) (-\chi_{\text{TRS}} \cos \alpha + i \chi_{\text{int}} \sin \alpha) \\ &= -\varepsilon_0 \mathcal{E}^3 \cos 2\alpha (\chi_{\text{TRS}} \cos \alpha - i \chi_{\text{int}} \sin \alpha). \end{aligned} \quad (60)$$

Using equations (59) and (60), the Stokes parameters can be calculated as,

$$\begin{aligned}
S_1 &\propto |P_x|^2 - |P_y|^2 \\
&= \mathcal{E}^6 \cos^2 2\alpha [(\chi_{\text{int}} \cos \alpha + i\chi_{\text{TRS}} \sin \alpha)(\chi_{\text{int}}^* \cos \alpha - i\chi_{\text{TRS}}^* \sin \alpha) \\
&\quad - (\chi_{\text{TRS}} \cos \alpha - i\chi_{\text{int}} \sin \alpha)(\chi_{\text{TRS}}^* \cos \alpha + i\chi_{\text{int}}^* \sin \alpha)] \\
&= \mathcal{E}^6 \cos^3 2\alpha (|\chi_{\text{int}}|^2 - |\chi_{\text{TRS}}|^2)
\end{aligned} \tag{61}$$

$$\begin{aligned}
S_2 &\propto \text{Re}\{P_x P_y^*\} \\
&= -\mathcal{E}^6 \cos^2 2\alpha [(\chi_{\text{int}} \cos \alpha + i\chi_{\text{TRS}} \sin \alpha)(\chi_{\text{TRS}}^* \cos \alpha + i\chi_{\text{int}}^* \sin \alpha) \\
&\quad + (\chi_{\text{int}}^* \cos \alpha - i\chi_{\text{TRS}}^* \sin \alpha)(\chi_{\text{TRS}} \cos \alpha - i\chi_{\text{int}} \sin \alpha)] \\
&= -\mathcal{E}^6 \cos^3 2\alpha (\chi_{\text{int}} \chi_{\text{TRS}}^* + \chi_{\text{TRS}} \chi_{\text{int}}^*) .
\end{aligned} \tag{62}$$

From this, the angle of rotation of the ellipse θ can be calculated as

$$\tan 2\theta = \frac{S_2}{S_1} = -2 \frac{\text{Re}(\chi_{\text{int}} \chi_{\text{TRS}}^*)}{|\chi_{\text{int}}|^2 - |\chi_{\text{TRS}}|^2} \stackrel{(51),(55)}{=} \frac{-2\Delta_{\text{gap}}^{\pm K} \text{Im}\Delta_{\omega}}{|\Delta_{\omega}|^2 - |\Delta_{\text{gap}}^{\pm K}|^2} \tag{63}$$

$$= \frac{-\frac{3\mathcal{E}^2 d^2}{16\Delta} \sin 2\alpha (\hbar/T_2)}{(2\Delta - 3\hbar\omega + \frac{9\mathcal{E}^2 d^2}{32\Delta})^2 + (\hbar/T_2)^2 - (\frac{3\mathcal{E}^2 d^2}{32\Delta})^2 \sin^2 2\alpha} . \tag{64}$$

For a small electric field, $\mathcal{E}^2 d^2 / (\hbar\Delta/T_2) \ll 1$, the TRS breaking $|\Delta_{\text{gap}}^{\pm K}| \ll |\Delta_{\omega}|$ and, thus, the rotation of the TH signal is linear in $\Delta_{\text{gap}}^{\pm K}$ and the intensity:

$$\tan 2\theta = - \frac{2}{1 + (2\Delta - 3\hbar\omega)^2 / (\hbar/T_2)^2} \frac{\Delta_{\text{gap}}^{\pm K}}{\hbar/T_2} \tag{65}$$

$$= - \frac{3}{16} \sin 2\alpha \frac{1}{1 + (2\Delta - 3\hbar\omega)^2 / (\hbar/T_2)^2} \frac{\mathcal{E}^2 d^2}{\hbar\Delta/T_2} . \tag{66}$$

Model Hamiltonian for bilayer TMDs

The classical/macroscopic approach (S3) shows that the TH rotation is identical in TMD AB-stacked bilayers and monolayers. To reproduce this result with our quantum mechanical model, we use an eight-band Hamiltonian for the TMD bilayer, where the first four basis states are located in the upper layer ‘u’, and the remaining basis sets are located in the lower layer ‘l’. The Hamiltonian is applicable near the $\pm K$ points of the Brillouin zone and

reads [21]

$$h(\mathbf{k}) = \begin{pmatrix} \Delta + \Delta E_{C_{\uparrow}^u} & 0 & \gamma^* f^*(\mathbf{k}) & 0 & 0 & 0 & 0 & 0 \\ 0 & \Delta + \Delta E_{C_{\downarrow}^u} & 0 & \gamma^* f^*(\mathbf{k}) & 0 & 0 & 0 & 0 \\ \gamma f(\mathbf{k}) & 0 & -\Delta + \tau\lambda + \Delta E_{V_{\uparrow}^u} & 0 & 0 & 0 & t_{\perp} & 0 \\ 0 & \gamma f(\mathbf{k}) & 0 & -\Delta - \tau\lambda + \Delta E_{V_{\downarrow}^u} & 0 & 0 & 0 & t_{\perp} \\ 0 & 0 & 0 & 0 & \Delta + \Delta E_{C_{\uparrow}^l} & 0 & \gamma f(\mathbf{k}) & 0 \\ 0 & 0 & 0 & 0 & 0 & \Delta + \Delta E_{C_{\downarrow}^l} & 0 & \gamma f(\mathbf{k}) \\ 0 & 0 & t_{\perp} & 0 & \gamma^* f^*(\mathbf{k}) & 0 & -\Delta - \tau\lambda + \Delta E_{V_{\uparrow}^l} & 0 \\ 0 & 0 & 0 & t_{\perp} & 0 & \gamma^* f^*(\mathbf{k}) & 0 & -\Delta + \tau\lambda + \Delta E_{V_{\downarrow}^l} \end{pmatrix} \quad (67)$$

where $\Delta E_{n_{\sigma}^{\varepsilon}}$ are the TRS breaking terms due to the OS and BS effects at the $\pm K$ points, given in equation (36). For simplicity and following the analysis in Ref. [22], we set the interlayer coupling to zero ($t_{\perp} = 0$), since $t_{\perp} \ll \lambda$, where λ is the energy difference in the valence band due to spin-orbit coupling. We then compute the eigenstates of the unperturbed Hamiltonian ($\Delta E_{n_{\sigma}^{\varepsilon}} = 0$). The valence band states are

$$|V_{\uparrow}^u\rangle = \begin{pmatrix} -\frac{\gamma^* f^*}{2\Delta - \tau\lambda} \\ 0 \\ 1 \\ 0 \\ 0 \\ 0 \\ 0 \\ 0 \end{pmatrix}, \quad |V_{\downarrow}^l\rangle = \begin{pmatrix} 0 \\ 0 \\ 0 \\ 0 \\ 0 \\ -\frac{\gamma f}{2\Delta - \tau\lambda} \\ 0 \\ 1 \end{pmatrix}, \quad |V_{\downarrow}^u\rangle = \begin{pmatrix} 0 \\ -\frac{\gamma^* f^*}{2\Delta + \tau\lambda} \\ 0 \\ 1 \\ 0 \\ 0 \\ 0 \\ 0 \end{pmatrix}, \quad |V_{\uparrow}^l\rangle = \begin{pmatrix} 0 \\ 0 \\ 0 \\ 0 \\ -\frac{\gamma f}{2\Delta + \tau\lambda} \\ 0 \\ 1 \\ 0 \end{pmatrix},$$

with spin-orbit split eigenvalues that depend on the valley index τ ,

$$\varepsilon_{V_{\uparrow}^u} = \varepsilon_{V_{\downarrow}^l} = -\Delta + \tau\lambda, \quad (68)$$

$$\varepsilon_{V_{\downarrow}^u} = \varepsilon_{V_{\uparrow}^l} = -\Delta - \tau\lambda. \quad (69)$$

The conduction band states are

$$|C_{\uparrow}^u\rangle = \begin{pmatrix} 1 \\ 0 \\ \frac{\gamma f}{2\Delta - \tau\lambda} \\ 0 \\ 0 \\ 0 \\ 0 \\ 0 \end{pmatrix}, \quad |C_{\downarrow}^u\rangle = \begin{pmatrix} 0 \\ 1 \\ 0 \\ \frac{\gamma f}{2\Delta + \tau\lambda} \\ 0 \\ 0 \\ 0 \\ 0 \end{pmatrix}, \quad |C_{\uparrow}^l\rangle = \begin{pmatrix} 0 \\ 0 \\ 0 \\ 0 \\ 1 \\ 0 \\ \frac{\gamma^* f^*}{2\Delta + \tau\lambda} \\ 0 \end{pmatrix}, \quad |C_{\downarrow}^l\rangle = \begin{pmatrix} 0 \\ 0 \\ 0 \\ 0 \\ 0 \\ 1 \\ 0 \\ \frac{\gamma^* f^*}{2\Delta - \tau\lambda} \end{pmatrix},$$

with eigenvalues

$$\varepsilon_{C_{\uparrow}^u} = \varepsilon_{C_{\downarrow}^u} = \varepsilon_{C_{\uparrow}^l} = \varepsilon_{C_{\downarrow}^l} = \Delta. \quad (70)$$

Evaluating $\chi^{(3)}$ for bilayer TMDs

In order to evaluate $\chi^{(3)}$ for the bilayer, can now evaluate the dipole matrix elements for the above mentioned eigenstates,

$$\begin{aligned} d_{C_{\uparrow}^u V_{\uparrow}^u}^x &= iq \langle C_{\uparrow}^u | \frac{\partial}{\partial k_x} | V_{\uparrow}^u \rangle = \frac{aq\gamma^*}{2\Delta - \lambda\tau} f_x^*, \\ d_{C_{\uparrow}^u V_{\uparrow}^u}^y &= iq \langle C_{\uparrow}^u | \frac{\partial}{\partial k_x} | V_{\uparrow}^u \rangle = \frac{aq\gamma^*}{2\Delta - \lambda\tau} f_y^*, \\ d_{C_{\downarrow}^u V_{\downarrow}^u}^x &= iq \langle C_{\uparrow}^u | \frac{\partial}{\partial k_x} | V_{\uparrow}^u \rangle = \frac{aq\gamma^*}{2\Delta + \lambda\tau} f_x^*, \\ d_{C_{\downarrow}^u V_{\downarrow}^u}^y &= iq \langle C_{\uparrow}^u | \frac{\partial}{\partial k_x} | V_{\uparrow}^u \rangle = \frac{aq\gamma^*}{2\Delta + \lambda\tau} f_y^*, \\ d_{C_{\uparrow}^l V_{\uparrow}^l}^x &= iq \langle C_{\uparrow}^u | \frac{\partial}{\partial k_x} | V_{\uparrow}^u \rangle = -\frac{aq\gamma}{2\Delta + \lambda\tau} f_x, \\ d_{C_{\uparrow}^l V_{\uparrow}^l}^y &= iq \langle C_{\uparrow}^u | \frac{\partial}{\partial k_x} | V_{\uparrow}^u \rangle = -\frac{aq\gamma}{2\Delta + \lambda\tau} f_y, \\ d_{C_{\downarrow}^l V_{\downarrow}^l}^x &= iq \langle C_{\uparrow}^u | \frac{\partial}{\partial k_x} | V_{\uparrow}^u \rangle = -\frac{aq\gamma}{2\Delta - \lambda\tau} f_x, \\ d_{C_{\downarrow}^l V_{\downarrow}^l}^y &= iq \langle C_{\uparrow}^u | \frac{\partial}{\partial k_x} | V_{\uparrow}^u \rangle = -\frac{aq\gamma}{2\Delta - \lambda\tau} f_y. \end{aligned} \quad (71)$$

where we have defined f_x and f_y already for the monolayer (50). We thus have the following relations:

$$\begin{aligned}
d_{C_{\uparrow}^u V_{\uparrow}^u}^y &= i\tau d_{C_{\uparrow}^u V_{\uparrow}^u}^x, \\
d_{C_{\downarrow}^u V_{\downarrow}^u}^y &= i\tau d_{C_{\downarrow}^u V_{\downarrow}^u}^x, \\
d_{C_{\uparrow}^l V_{\uparrow}^l}^y &= -i\tau d_{C_{\uparrow}^l V_{\uparrow}^l}^x, \\
d_{C_{\downarrow}^l V_{\downarrow}^l}^y &= -i\tau d_{C_{\downarrow}^l V_{\downarrow}^l}^x.
\end{aligned} \tag{72}$$

The above dipole terms and their complex conjugates are the only elements of the dipole matrix that are non-zero, simplifying analytical calculations of $\chi^{(3)}$.

Evaluating $\chi_{dcba}^{(3)}$ for the bilayer from equation (38) at the resonant $\pm K$ points using the band energies (68), (69), (70) and the dipoles (71), we find that the expression simplifies to evaluating (43) summed over the above c and v . This means that

$$\begin{aligned}
\frac{\chi_{dcba}^{(3)}}{C} &= \mathcal{P}_I \sum_{(c,v)} \sum_{\mathbf{k}} \frac{-d_{vc}^d(\mathbf{k}) d_{cv}^c(\mathbf{k})}{(\varepsilon_{cv}(\mathbf{k}) - 3\hbar\omega + i\hbar/T_2)\hbar\omega} \left(\frac{d_{cv}^a(\mathbf{k}) d_{vc}^b(\mathbf{k})}{\varepsilon_{cv}(\mathbf{k}) - \hbar\omega} + \frac{d_{vc}^a(\mathbf{k}) d_{cv}^b(\mathbf{k})}{\varepsilon_{vc}(\mathbf{k}) - \hbar\omega} \right) \\
&\quad - \frac{d_{vc}^d(\mathbf{k})}{\varepsilon_{cv}(\mathbf{k}) - 3\omega + i\hbar/T_2} \frac{\partial}{\partial k_c} \left[\frac{1}{\varepsilon_{cv}(\mathbf{k}) - 2\omega} \frac{\partial}{\partial k_b} \left(\frac{d_{cv}^a(\mathbf{k}) f_{vc}}{\varepsilon_{cv}(\mathbf{k}) - \omega} \right) \right], \tag{73}
\end{aligned}$$

where the first summation is over the (c, v) pairs for which the dipole moment is non-zero (71). Calculating $\chi_{xxxx}^{(3)}$, we get

$$\chi_{xxxx}^{(3)} = \frac{2\Delta_{\omega, \text{BL}}}{\Delta_{\omega, \text{BL}}^2 - (\Delta_{\text{BL}}^{\uparrow/\downarrow})^2} \mathcal{C}' = \chi_{\text{int}}^{\text{BL}}, \tag{74}$$

with

$$\Delta_{\omega, \text{BL}} := 2\Delta - \lambda - 3\hbar\omega + \frac{i\hbar}{T_2} + \frac{9\mathcal{E}^2 d_{\text{BL}}^2}{16(2\Delta - \lambda)}, \tag{75}$$

$$\Delta_{\text{BL}}^{\uparrow/\downarrow} := \frac{3\mathcal{E}^2 d_{\text{BL}}^2}{16(2\Delta - \lambda)} \sin 2\alpha \tag{76}$$

and,

$$\begin{aligned}
\mathcal{C}' := C &\frac{4a^4 |\gamma|^2 q^4}{\Delta(2\Delta - \lambda)^4 (2\Delta - \lambda - 2\omega)(2\Delta - \lambda + \omega)(2\Delta - \lambda - \omega)^2} \left[|\gamma|^2 (\omega (10\Delta^2 - 7\Delta\lambda + \lambda^2) \right. \\
&\quad \left. + (\Delta - \lambda)(2\Delta - \lambda)^2 - 2\Delta\omega^2) + 3\Delta\zeta_3(2\Delta - \lambda)^2 ((2\Delta - \lambda)^2 - \omega^2) \right]. \tag{77}
\end{aligned}$$

Similarly, evaluating $\chi_{xyyy}^{(3)}$, we get

$$\chi_{xyyy}^{(3)} = \frac{2i\Delta_{\text{BL}}^{\uparrow/\downarrow}}{\Delta_{\omega, \text{BL}}^2 - (\Delta_{\text{BL}}^{\uparrow/\downarrow})^2} \mathcal{C}' = \chi_{\text{TRS}}^{\text{BL}}. \quad (78)$$

Just as in the monolayer, it is possible by evaluating equation (73) to validate that the relations for the $\bar{3}m'$ magnetic point group are fulfilled (detailed calculation not shown):

$$\begin{aligned} \chi_{xxxx}^{(3)} &= \chi_{yyyy}^{(3)} = 3\chi_{xxyy}^{(3)} = 3\chi_{xyyx}^{(3)} = 3\chi_{xyxy}^{(3)} \equiv \chi_{\text{int}}^{\text{BL}} \\ \chi_{xyyy}^{(3)} &= 3\chi_{xxxy}^{(3)} = 3\chi_{xxyx}^{(3)} = 3\chi_{xyxx}^{(3)} = -3\chi_{yyyx}^{(3)} = -3\chi_{yyxy}^{(3)} = -3\chi_{yxyy}^{(3)} = -\chi_{yxxx}^{(3)} \equiv \chi_{\text{TRS}}^{\text{BL}}. \end{aligned}$$

Evaluation of the third-harmonic rotation from the $\chi^{(3)}$ tensor

We shall now evaluate the TH rotation using the $\chi^{(3)}$ tensor by evaluating the Stokes parameters as in equation (63).

$$\tan 2\theta = \frac{S_2}{S_1} = -2 \frac{\text{Re}(\chi_{\text{int}}^{\text{BL}}(\chi_{\text{TRS}}^{\text{BL}})^*)}{|\chi_{\text{int}}^{\text{BL}}|^2 - |\chi_{\text{TRS}}^{\text{BL}}|^2} \stackrel{(74),(78)}{=} \frac{-2\Delta_{\text{BL}}^{\uparrow/\downarrow} \text{Im}(\Delta_{\omega, \text{BL}})}{|\Delta_{\omega, \text{BL}}|^2 - |\Delta_{\text{BL}}^{\uparrow/\downarrow}|^2} \quad (79)$$

$$= \frac{-\frac{3\mathcal{E}^2 d_{\text{BL}}^2}{8(2\Delta - \lambda)} \sin 2\alpha (\hbar/T_2)}{\left(2\Delta - \lambda - 3\hbar\omega + \frac{9\mathcal{E}^2 d_{\text{BL}}^2}{16(2\Delta - \lambda)}\right)^2 + (\hbar/T_2)^2 - \left(\frac{3\mathcal{E}^2 d_{\text{BL}}^2}{16(2\Delta - \lambda)}\right)^2 \sin^2 2\alpha}. \quad (80)$$

As for the monolayer, for a small electric field, $\mathcal{E}^2 d_{\text{BL}}^2 / (2\Delta - \lambda) \ll \hbar/T_2$, the TRS breaking $|\Delta_{\text{BL}}^{\uparrow/\downarrow}| \ll |\Delta_{\omega, \text{BL}}|$ and, thus, the rotation of the TH polarization is linear in $\Delta_{\text{BL}}^{\uparrow/\downarrow}$ and the intensity:

$$\tan 2\theta = -\frac{2}{1 + (2\Delta - \lambda - 3\hbar\omega)^2 / (\hbar/T_2)^2} \frac{\Delta_{\text{BL}}^{\uparrow/\downarrow}}{\hbar/T_2} \quad (81)$$

$$= -\frac{3}{8} \sin 2\alpha \frac{1}{1 + (2\Delta - \lambda - 3\hbar\omega)^2 / (\hbar/T_2)^2} \frac{\mathcal{E}^2 d_{\text{BL}}^2}{\hbar(2\Delta - \lambda)/T_2}. \quad (82)$$

Note that the parameter $2\Delta - \lambda$ corresponds to 2Δ in the monolayer, because of the neglect of spin-orbit coupling in the two-band model for the monolayer. Also note, that the bilayer dipole then equals the monolayer dipole.

S7 EXEMPLARY POLAR PLOTS OF THE FUNDAMENTAL AND THIRD-HARMONIC BEAMS

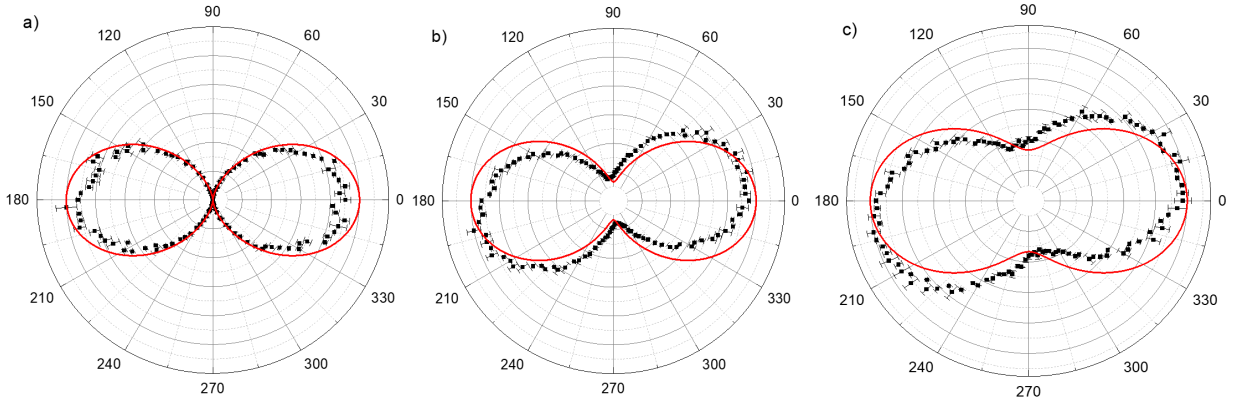


Fig. S4: Exemplary polar plots of the fundamental (solid red line) and emitted TH (black squares) beams for WS_2 monolayer excited at resonance with the A1s exciton, *i.e.*, fundamental beam at 1830 nm for ellipticity angles of a) linear, b) -20° and c) -30°

S8 NONLINEAR FARADAY ROTATION FOR MO BASED TMDs

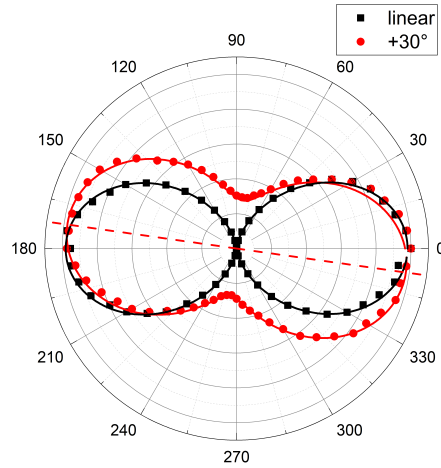


Fig. S5: Nonlinear Faraday rotation for MoSe_2 monolayer. For linear excitation (black squares) the polarization of the emitted TH is parallel to the input, while for an ellipticity angle of $+30^\circ$ (red circles) the polarization of the TH is rotated by -8°

While Mo based TMDs are known to have a much lower degree of valley polarization,

which is not visible in photoluminescence experiments at room temperature, our method does not rely on the dynamics of excitons and/or real populations of charge carriers. In contrast, we measure an all-optically induced broken TRS, which occurs within the pulse duration. Therefore, we expect to see a nonlinear Faraday rotation also for Mo based TMDs. To confirm this, we performed similar experiments on a MoSe₂ monolayer (Fig. S5), where we set the fundamental wavelength to 2340 nm (resonant with the A1s exciton) and the input pulse energy to ~ 130 pJ. Under these experimental conditions, we observe a nonlinear Faraday rotation of -8° upon changing the polarization of the fundamental beam from linear (black squares) to an ellipticity angle of $+30^\circ$ (red circles).

S9 COMPARISON LINEAR TRANSMITTANCE AND THIRD-HARMONIC WAVELENGTH DEPENDENCE

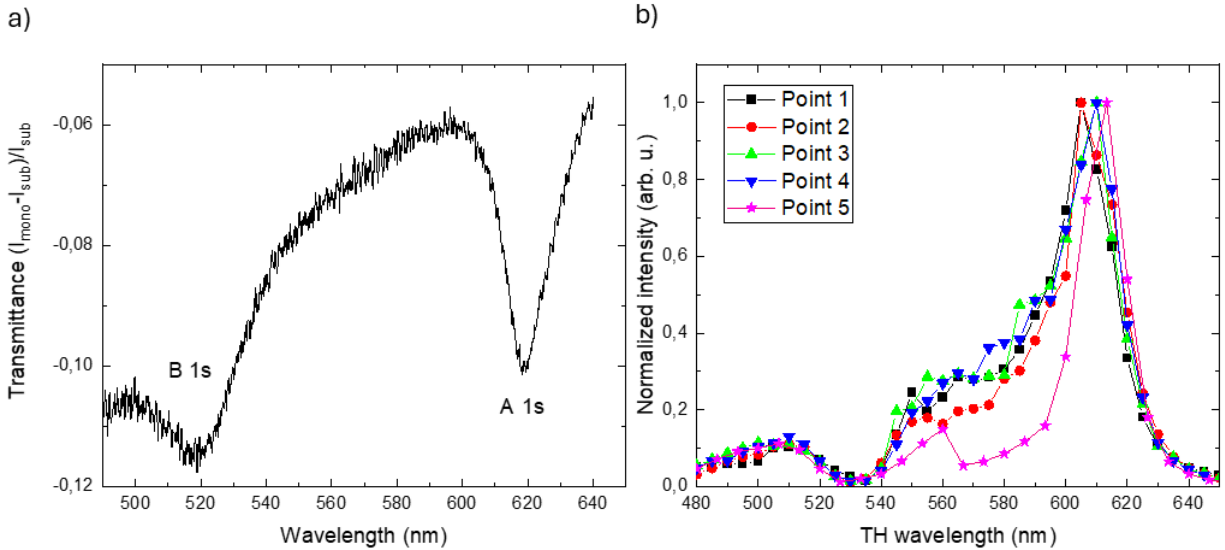


Fig. S6: Linear and nonlinear characterization of the WS₂ monolayer: a) Linear transmittance. The B1s and A1s excitons are clearly visible. b) Normalized intensity of the TH wavelength dependence for five different sample positions.

-
- [1] Fecher, G. H., Kübler, J. & Felser, C. Chirality in the solid state: Chiral crystal structures in chiral and achiral space groups. *Materials* **15** (2022). URL <https://www.mdpi.com/>

- 1996–1944/15/17/5812.
- [2] Padmanabhan, H., Munro, J. M., Dabo, I. & Gopalan, V. Antisymmetry: Fundamentals and applications. *Annual Review of Materials Research* **50**, 255–281 (2020). URL <https://www.annualreviews.org/content/journals/10.1146/annurev-matsci-100219-101404>.
 - [3] Fiebig, M. *Nonlinear Optics on Ferroic Materials* (Wiley, 2023).
 - [4] Lifshitz, R. Magnetic point groups and space groups. *Encyclopedia of Condensed Matter Physics*, Ed. F. Bassani, G.L. Liedl, and P. Wyder, **3**, 219–226 (2005).
 - [5] Dresselhaus, M. S., Dresselhaus, G. & Jorio, A. *Group theory: application to the physics of condensed matter* (Springer Science & Business Media, 2007).
 - [6] Curie, P. Sur la symétrie dans les phénomènes physiques, symétrie d’un champ électrique et d’un champ magnétique. *J. Phys. Theor. Appl.* **3**, 393–415 (1894). URL <https://hal.science/jpa-00239814>.
 - [7] Rodríguez-Carvajal, J. & Bourée, F. Symmetry and magnetic structures. *EPJ Web of Conferences* **22**, 00010 (2012). URL <https://doi.org/10.1051/epjconf/20122200010>.
 - [8] Graef, M. D. Teaching crystallographic and magnetic point group symmetry using three-dimensional rendered visualizations. URL <https://www.iucr.org/education/pamphlets/23/full-text>.
 - [9] Boyd, R. W. Chapter 1 - the nonlinear optical susceptibility. In Boyd, R. W. (ed.) *Nonlinear Optics (Fourth Edition)*, 1–64 (Academic Press, 2020), fourth edition edn. URL <https://www.sciencedirect.com/science/article/pii/B9780128110027000102>.
 - [10] <https://www.cryst.ehu.es/cgi-bin/cryst/programs/mtensor.pl>. Accessed on 10.02.2025.
 - [11] Gallego, S. V., Etxebarria, J., Elcoro, L., Tasci, E. S. & Perez-Mato, J. M. Automatic calculation of symmetry-adapted tensors in magnetic and non-magnetic materials: a new tool of the Bilbao Crystallographic Server. *Acta Crystallographica Section A* **75**, 438–447 (2019). URL <https://doi.org/10.1107/S2053273319001748>.
 - [12] Hecht, E. *Optik* (Oldenbourg, 2005), 4th edn.
 - [13] Bloembergen, N. Conservation laws in nonlinear optics. *J. Opt. Soc. Am.* **70**, 1429–1436 (1980). URL <https://opg.optica.org/abstract.cfm?URI=josa-70-12-1429>.
 - [14] Herrmann, P. *et al.* Nonlinear all-optical coherent generation and read-out of valleys in atomically thin semiconductors. *Small* **19**, 2301126 (2023).

- URL <https://onlinelibrary.wiley.com/doi/abs/10.1002/sml.202301126>.
<https://onlinelibrary.wiley.com/doi/pdf/10.1002/sml.202301126>.
- [15] Sie, E. J. *et al.* Large, valley-exclusive Bloch-Siegert shift in monolayer WS₂. *Science* **355**, 1066–1069 (2017). URL <https://www.science.org/doi/abs/10.1126/science.aal2241>.
<https://www.science.org/doi/pdf/10.1126/science.aal2241>.
 - [16] Herrmann, P. *et al.* Nonlinear valley selection rules and all-optical probe of broken time-reversal symmetry in monolayer wse2. *Nature Photonics* **19**, 300–306 (2025). URL <https://doi.org/10.1038/s41566-024-01591-z>.
 - [17] Le Kien, F., Schneeweiss, P. & Rauschenbeutel, A. Dynamical polarizability of atoms in arbitrary light fields: general theory and application to cesium. *The European Physical Journal D* **67**, 92 (2013).
 - [18] Aversa, C. & Sipe, J. E. Nonlinear optical susceptibilities of semiconductors: Results with a length-gauge analysis. *Phys. Rev. B* **52**, 14636–14645 (1995). URL <https://link.aps.org/doi/10.1103/PhysRevB.52.14636>.
 - [19] Taghizadeh, A. & Pedersen, T. G. Nonlinear optical selection rules of excitons in monolayer transition metal dichalcogenides. *Phys. Rev. B* **99**, 235433 (2019). URL <https://link.aps.org/doi/10.1103/PhysRevB.99.235433>.
 - [20] Korolev, V. *et al.* Unveiling the role of electron-phonon scattering in dephasing high-order harmonics in solids (2024). URL <https://arxiv.org/abs/2401.12929>. 2401.12929.
 - [21] Gong, Z. *et al.* Magnetoelectric effects and valley-controlled spin quantum gates in transition metal dichalcogenide bilayers. *Nature communications* **4**, 2053 (2013).
 - [22] Jones, A. M. *et al.* Spin–layer locking effects in optical orientation of exciton spin in bilayer WSe₂. *Nature Physics* **10**, 130–134 (2014). URL <https://doi.org/10.1038/nphys2848>.